Rawnaq Jima'a[1], Naser Shaalan[2], Muna Bufaroosha[3], Gamal A. El-Hiti[4], Benson M. Kariuki[5], Dina S. Ahmed[6], Emad Yousif[7**]*

[1]*Department of Chemistry, College of Science, University of Diyala, Diyala, Iraq;* [2]*Department of Chemistry, College of Science for Women, University of Baghdad, Baghdad, Iraq;* [3]*Department of Chemistry, College of Science, United Arab Emirates University, Al-Ain, United Arab Emirates;* [4]*Department of Optometry, College of Applied Medical Sciences, King Saud University, Riyadh, Saudi Arabia;* [5]*School of Chemistry, Cardiff University, Main Building, Park Place, Cardiff, UK;* [6]*Department of Chemical Industries, Institute of Technology-Baghdad, Middle Technical University, Baghdad, Iraq;* [7] *Department of Chemistry, College of Science, Al-Nahrain University, Baghdad, Iraq*

Synthesis and Properties of New Metal Complexes Containing Heterocyclic Moieties and Investigation of the Role of the Metal in Carbon Dioxide Gas Capture

ABSTRACT

The continuous release of carbon dioxide (CO_2) into the atmosphere will inevitably lead to greater environmental damage. The capture and storage of CO_2 is one strategy to mitigate the harm associated with its high concentrations in the atmosphere. The design and synthesis of new materials to act as storage media for CO_2 is currently an important challenge for researchers. In this regard, the investigation into the synthesis of new organometallic materials and their potential as CO_2 storage media is reported. Therefore, the current work aimed to produce new materials using a simple procedure and investigate their properties, including factors affecting their CO_2 adsorption. Four metal complexes containing heterocyclic units were synthesized using a simple method, and their structures were confirmed using several techniques. The surface morphology of the materials was inspected by microscopy. The metal complexes exhibited tunable particle sizes with diameters that ranged from 16.77 to 97.62 nm and a Brunauer–Emmett–Teller surface area of 1.20–4.01 m^2/g. The materials can capture CO_2 at 323 K and 40 bars, with the manganese-containing complex showing the highest CO_2 storage capacity (13.1 cm^3/gm).

Keywords: *synthesis, metal complexes, carbon dioxide capture, surface area, surface morphology*

1. INTRODUCTION

The level of carbon dioxide (CO_2) in the atmosphere is on an upward curve correlated with the growing demand for energy and resources (e.g., power stations and the pharmaceutical industry) and the associated high demand for fossil fuels [1]. Currently, the concentration of CO_2 in the atmosphere is over 50% higher than the level at the end of the 19th century [2]. The increase in CO_2 levels is linked to rises in the surface temperature of the Earth, sea level, and the acidity of ocean water, for example, leading to serious environmental and socioeconomic problems [3–6]. It is challenging to reduce CO_2 emissions into the atmosphere rapidly due to the continuous high demand for fossil fuels, and so a multifaceted strategy is needed to control the levels. One approach is to find reliable alternative sources of energy to replace the use of fossil fuels, and, indeed, much attention has been paid to renewable sources such as wind, solar, nuclear, and biomass as a strategy to reduce CO_2 emissions into the atmosphere [7, 8]. However, renewable sources currently fall far short of the capacity required to meet the global demand for energy and generally cannot compete with fossil fuels in terms of cost [9].

Another way to address the unsustainable levels of the gas in the atmosphere is CO_2 capture. For this to be successful, the design and use of new adsorbent materials to capture CO_2 requires exploration [10–13]. Several processes have been used

to capture CO_2 from the atmosphere [14–20]. For example, amines (e.g., ethanolamine and ammonia) have been employed to remove CO_2 from natural gas [21]. However, there are associated risks with the use of amines since they are volatile and hazardous. The process of CO_2 capture often involves the separation of the gas and its adsorption at high pressure [22]. Thus, many new porous materials have been tested as storage media [23, 24]. Porous materials designed for CO_2 capture should meet certain requirements; they should be stable, polar, have large enough surface area and pore size, be easy to synthesize, be cheap to produce, have a long shelf life, be recyclable, and not pose a danger to the environment [25–28]. Examples of materials that have been tested as CO_2 adsorbents include metal-organic frameworks, carbon-based materials, zeolites, cross-linked polymers, and inorganic materials [29–32]. Metal oxides have been used with metal carbonates as materials in a chemical looping process, but their adsorption capacity is limited [33,34]. Additionally, carbon materials (e.g., activated carbons) are not suitable for flue gases due to their hydrophilic properties and poor selectivity [35–39]. Porous materials, including organic polymers, are used as CO_2 adsorbents due to their low heat of adsorption and high surface area [40–42]. However, the synthetic procedures for these materials are not environmentally friendly [43].

Organometallic compounds (e.g., metal–organic frameworks) have been used in many applications, such as storage and separation media, catalysts, and sensors [44]. However, there are problems associated with the use of organometallics that need to be addressed to enable their commercialization. The most common issues are their toxicity, regeneration, and reuse. Some success has been reported with organometallic regeneration and reuse [44]. However, further research is still needed to improve materials efficiency, cost of production, cleanliness, and simplicity of the process. Recently, success has been achieved in capturing CO_2 using polymeric materials [45–47], heterocycles [48,49], and organometallics [50–53]. Heterocycles such as thiophenes have useful applications in medicine, optoelectronic conductive devices, catalysis, and the production of dyes, plasticizers, and resins [54,55]. The current work explores the synthesis of new complexes containing different metals and heterocyclic units, such as thiophene. While recognizing that they do not show the levels required for application, an additional aim is to use the compounds as a model to explore how the metal identity influences the CO_2 absorption in such materials.

EXPERIMENTAL

General

Chemicals, solvents, and reagents (analytical grades) were obtained from Merck (Gillingham, UK) and used as received. Melting points were measured on a Gallenkamp melting point apparatus. The FTIR spectra (KBr disks) were recorded on a Shimadzu IR Prestige-21 single-beam Fourier Transform Infrared spectrophotometer (400–4000 cm^{-1}). A Shimadzu-1800 double-beam UV-Vis spectroscopy was used to record the electronic absorption spectra (200–1100 nm; 10^{-3} M in DMF). A Bruker BM6 magnetic monitor was used to measure the magnetic susceptibility of complexes. Molar conductance (10^{-3} M in DMF) was calculated using a WTW ProfiLine Oxi3205 conventional portable meter. The NMR spectra were recorded on Bruker DRX300N-MR spectrometry in DMSO-d_6. The electron impact (70 eV) mass spectrum of the ligand was conducted on a Shimadzu GCMS-QP2010-plus mass spectrometer that was equipped with a DB-5MS column (30 m × 0.25 mm I.D. × 0.1 μm). The injector temperature was kept at 260 °C, and the oven temperature started at 50 °C for 2 minutes, increased to 210 °C (3 °C/min), and then to 270 °C (10 °C/min). The carrier gas used was helium, with a pressure of 69 kPa. The complexes were dried for 4 hours at 60 °C using a vacuum oven to dry samples. The specific surface area of complexes was measured using the Brunauer-Emmett-Teller (BET) method. Pore sizes and volumes were measured via the Barrett–Joyner–Halenda (BJH) method. The CO_2 uptake measurements (three times) were performed on an H-sorb 2600 high-pressure volumetric adsorption instrument. The complex (1 g) was first degassed for 1 h at 50 °C in a vacuum oven to remove any traces of either water or solvent that are trapped within the pores of the complexes. Based on our previous work, the pressure and the temperature were set at 40 bar and 323 K, respectively [48–50]. The gas uptake experiment was then replicated three times under identical conditions to determine the optimum pressure. A ZEISS Sigma VP (10 kV) was used to record the field emission scanning electron microscopy (FESEM) images. The energy dispersive x-ray (EDX) and mapping tests for the complexes were performed on Oxford Instruments equipment.

A Veeco instrument was used to record the atomic force microscopy (AFM) images.

Synthesis of 3-hydrazone-1,3-dihydroindole-2-one (2)

A solution of 1H-indole-2,3-dione (**1**; 1.00 g, 6.8 mmol) in MeOH (10 mL) was added dropwise to a stirred solution of hydrazine monohydrate (0.34 g,6.8 mmol) in MeOH (10 mL). The mixture was refluxed for 6 hours, and the yellow solid formed was filtered, washed with MeOH, and dried at 50 °C to give pure **2** (Scheme 1) in 80% yield, M.P. 187–188 °C. FTIR (cm^{-1}): 3369, 3197, 1689, 1560, 1461.
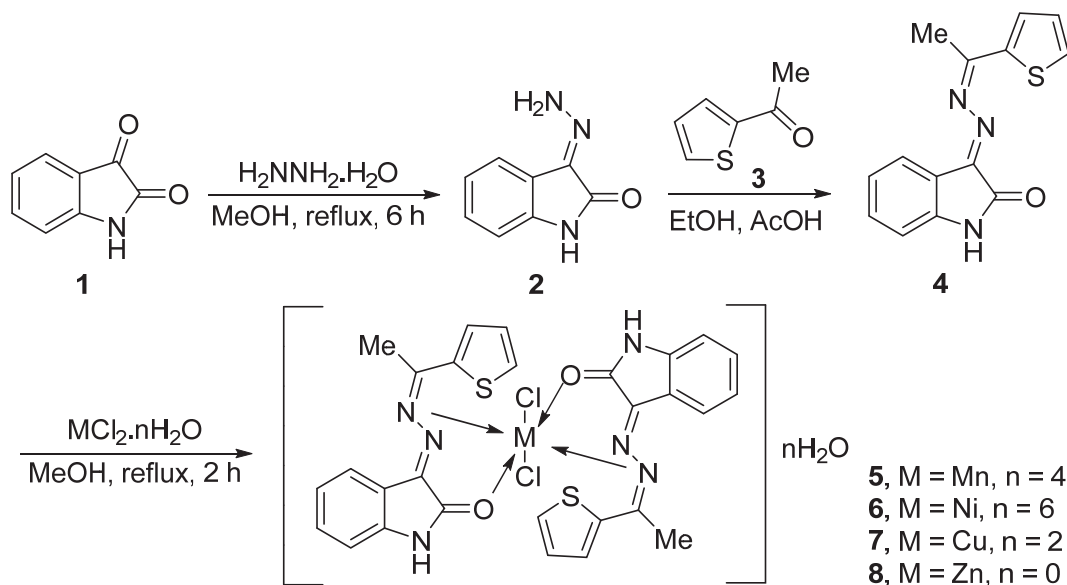
Scheme 1. Synthesis of metal complexes 5–8.

Synthesis of 3-[(1-Thiophen-2-yl-ethylidene) hydrazone]-1,3-dihydroindol-2-one (4)

A solution of **2** (1.00 g, 6.2 mmol) in EtOH (10 mL) was added dropwise to a stirred solution of 1-(thiophen-2-yl)ethan-1-one (**3**; 0.78 g, 6.2 mmol) in EtOH (10 mL) containing glacial AcOH (0.5 mL). The mixture was refluxed for 4 hours, and the orange solid formed was collected by filtration, washed with EtOH, recrystallized using a mixture of MeOH and EtOH (1:1 by volume), and dried at 50 °C to give pure **4** (Scheme 1) in 75% yield, M.P. 234–236 °C. FTIR (cm^{-1}): 3372, 3201, 1688, 1612, 1465. UV (nm): 249, 313. ^{1}H NMR (400 MHz; DMSO-d$_6$): 2.51 (s, 3H, Me), 6.86 (t, 8 Hz, 1H, Ar), 6.97 (t, 8 Hz, 1H, Ar), 7.16 (d, 8 Hz, 1H, Ar), 7.22 (d, 8 Hz, 1H, Ar), 8.56, (d, 5 Hz, 1H, thiophene), 8.75–8.78 (m, 2H, thiophene), 10.70 (s, 1H, NH). ^{13}C NMR (100 MHz; DMSO-d$_6$): 39.3, 110.1, 117.9, 121.8, 122.7, 123.2, 126.7, 127.5, 129.0, 129.2, 139.1, 141.0, 163.3, 166.4. EI-MS (m/z, %): 270 (M$^+$, 100), 197 (15), 160 (55).

Synthesis of metal complexes 5–8

A mixture of metal chloride (1.8 mmol) and **4** (0.97 g, 3.6 mmol) in MeOH (10 mL) was refluxed for 2 h. The colored complexes obtained were collected by filtration, washed with MeOH, and dried to give **5–8** (Scheme 1) in good yields (Table 1). The solids obtained are highly insoluble in most solvents, and therefore, no crystallization process was performed.

Table 1. Color, melting point, yield, and elemental analysis of metal complexes 5–8

Complex	Metal	Color	M.P (°C)	Yield (%)	Analysis (%); Found (Calculated)		
					C	H	M
5	Mn	Reddish brown	213–215	66	45.56 (45.66)	4.09 (4.11)	7.29 (7.46)
6	Ni	Yellow	200–203	65	43.20 (43.32)	4.37 (4.41)	7.37 (7.56)
7	Cu	Dark brown	177–179	60	47.31 (47.43)	3.65 (3.70)	8.87 (8.96)
8	Zn	Light yellow	218–221	75	49.74 (49.83)	3.34 (3.29)	9.52 (9.69)

Results and Discussion

Synthesis of metal complexes

Compound **4** was obtained in 75% yield, as shown in Scheme 1. The mass spectrum of **4** showed a pseudo molecular ion peak (MH$^+$) at m/z = 270. Its ^{1}H NMR spectrum showed the presence of the methyl and NH protons as singlet signals at 2.51 and 10.70 ppm, respectively. The ^{13}C NMR spectrum of **4** showed the carbonyl carbon at 166.4 ppm. The reaction of **4** with metal chlorides leads to the formation of metal complexes **5–8** (Scheme 1) in rea-

sonable yields (Table 1). The structures of **5–8** were confirmed by the FTIR (Table 2), electronic (Table 3), and NMR (Table 4) spectral data.

The coordination took place between the metal and oxygen rather than the sulfur. The lone pairs of electrons of the sulfur atom are involved in thiophene aromaticity and are not available for coordination. In addition, the high melting points of the synthesized complexes indicate their high stability in the air. The complexes decomposed at temperatures higher than 200 °C.

Table 2. Selected FTIR absorption bands (cm–1) of 5–8

Complex	Metal	OH	NH	C=O	C=N	M–N	M–O	M–Cl
5	Mn	3360	3161	1762	1658	524	501	289
6	Ni	3360	3163	1730	1658	524	501	289
7	Cu	3450	3196	1732	1618	480	457	277
8	Zn	—	3161	1691	1652	524	501	289

FTIR spectroscopy of 5–8.

The FTIR spectra of **5–8** showed the presence of absorption bands corresponding to the C=N bonds in thiophene that appeared in the regions of 1618–1658 cm^{-1} (Table 2). They also showed absorption bands that are corresponding to the carbonyl group at 1691–1730 cm^{-1}. There was a shift in the carbonyl group position compared with compound **4,** indicating that coordination has taken place. Indeed, new absorption bands corresponding to the M–N, M–O, and M–Cl bonds appeared in the regions of 480–534, 457–501, and 277–289 cm^{-1}, respectively [56, 57].

Molar conductivity, magnetic moment, and UV spectroscopy of 5–8

The electronic spectra (200–1100 nm) of **5–8** were measured in DMF at 20 °C. The UV spectrum of the Mn complex showed bands at 267 and 317 nm corresponding to the π–π* and n–π* transitions, respectively (Table 3). The spectrum does not show d–d transitions except a band at 395 nm, which was attributed to charge transfer (CT) since the multiplicities in the ground and excited states are different. This result is consistent with the magnetic moment

(μ_{eff} = 6.26 BM), indicating an octahedral geometry [58,59].

The UV spectrum of the Ni complex showed bands at 260 and 312 nm that were assigned to the π–π* and n–π* transitions, respectively. In addition, three bands in the visible region at 400, 500, and 810 nm were attributed to the spin-allowed transitions $^3A_2g(F)\rightarrow^3T_1g(P)$, $^3A_2g(F)\rightarrow^3T_1g(F)$, and $^3A_2g(F)\rightarrow^3T_2g(F)$, respectively.

The magnetic moment (2.68 BM) of the Ni complex was in the normal range for octahedral arrangement [58, 59]. For the Cu complex, three absorption bands appearing at 211, 268, and 380 nm were attributed to π–π*, n–π* transitions, and the CT, respectively. The broad band centered at 635 nm was attributed to $^2Eg\rightarrow^2T_2g$ transitions. The d–d bands were strongly indicative of the distorted octahedral geometry, which was confirmed by magnetic susceptibility (1.89 BM) [60].

The electronic spectrum of the Zn complex showed a charge transfer band at 407 nm as well as two bands at 275 and 329 nm due to π–π* and n–π* transitions, respectively [58]. The molar conductivity recorded indicates that complexes **5–8** are non-electrolytes.

Table 3. Molar conductivity, magnetic moment, and electronic spectral data of metal complexes 5–8

Complex	Metal	Conductivity (Ohm^{-1} cm^2 mol^{-1})	μeff (BM)	Band (nm)	Assignment
5	Mn	10	6.26	267	π–π^*
				317	n–π^*
				395	CT
6	Ni	20	3.68	260	π–π^*
				312	n–π^*
				400	$^3A_2g(F) \rightarrow {}^3T_1g(P)$
				500	$^3A_2g(F) \rightarrow {}^3T_1g(F)$
				800	$^3A_2g(F) \rightarrow {}^3T_2g(F)$
7	Cu	32	1.89	211	π–π^*
				268	n–π^*
				280	CT
				635	$^2Eg \rightarrow {}^2T_2g$
8	Zn	3	Diamagnetic	275	π–π^*
				329	n–π^*
				407	CT

NMR Spectroscopy of 5–8

The structures of **5–8** were confirmed by the NMR spectral data (Table 4). It was not possible to record the NMR spectrum of the Mn complex using the standard technique at room temperature due to its poor solubility in a variety of deuterated solvents [58,61]. The ^{1}H NMR spectra of the metal complexes showed the methyl protons as singlets in the 2.18–2.38 ppm region. In addition, the NH protons appeared as singlets at the 10.01–10.70 ppm region. The carbonyl carbons appeared downfield (166.2–168.6 ppm) in the ^{13}C NMR spectra, while the methyl carbons appeared at high field (27.2–27.8 ppm). It should be noted that the mass spectra of the synthesized complexes **5–8** were very poor and provided no useful information, presumably due to their low volatility.

Table 4. NMR spectral data of metal complexes 6–8

Complex	Metal	^{1}H NMR	^{13}C NMR
6	Ni	2.38 (s, 3H, Me), 6.79 (t, 8 Hz, 1H, Ar), 6.83 (t, 8 Hz, 1H, Ar), 6.99 (d, 8 Hz, 1H, Ar), 7.19 (d, 8 Hz, 1H, Ar), 8.60, (d, 4 Hz, 1H, thiophene), 8.82–8.87 (m, 2H, thiophene), 10.70 (s, 1H, NH)	27.3, 110.4, 117.8, 122.7, 126.7, 127.4, 129.2, 134.4. 135.4, 139.0, 144.5, 145.4, 163.2, 168.6
7	Cu	2.38 (s, 3H, Me), 6.72 (t, 8 Hz, 1H, Ar), 6.87 (t, 8 Hz, 1H, Ar), 7.14 (d, 8 Hz, 1H, Ar), 7.31 (d, 8 Hz, 1H, Ar), 8.65, (d, 4 Hz, 1H, thiophene), 8.72–8.77 (m, 2H, thiophene), 10.70 (s, 1H, NH)	27.8, 110.0, 112.6, 118.2, 121.6, 123.2, 125.1, 129.7, 133.1, 138.8, 144.5, 151.1, 159.8, 166.2
8	Zn	2.18 (s, 3H, Me), 6.82 (t, 8 Hz, 1H, Ar), 6.82 (t, 8 Hz, 1H, Ar), 6.91 (d, 8 Hz, 1H, Ar), 7.13 (d, 8 Hz, 1H, Ar), 7.91, (d, 4 Hz, 1H, thiophene), 8.69–8.79 (m, 2H, thiophene), 10.01 (s, 1H, NH)	27.2, 110.5, 117.9, 121.5, 122.7, 126.3, 127.5, 129.3, 134.3, 135.3, 139.1, 140.9, 163.3, 166.4

EDX Mapping of 5–8

The elemental contents of **5–8** were confirmed using the energy-dispersive X-ray analysis (EDX). The EDX images provide a rough estimate of metal contents. However, it is not as precise as the results obtained from the elemental analysis. Figure 1 shows the EDX mapping graphs for the synthesized metal complexes, and they reveal all the elements within the structures of metal complexes. Figure 1 showed a lower percentage for Zn compared with those shown for appeared for the other metals. It should be noted that the structures and quantity of water for the metal complexes (Scheme 1) were suggested based on the elemental analysis (Table 1).
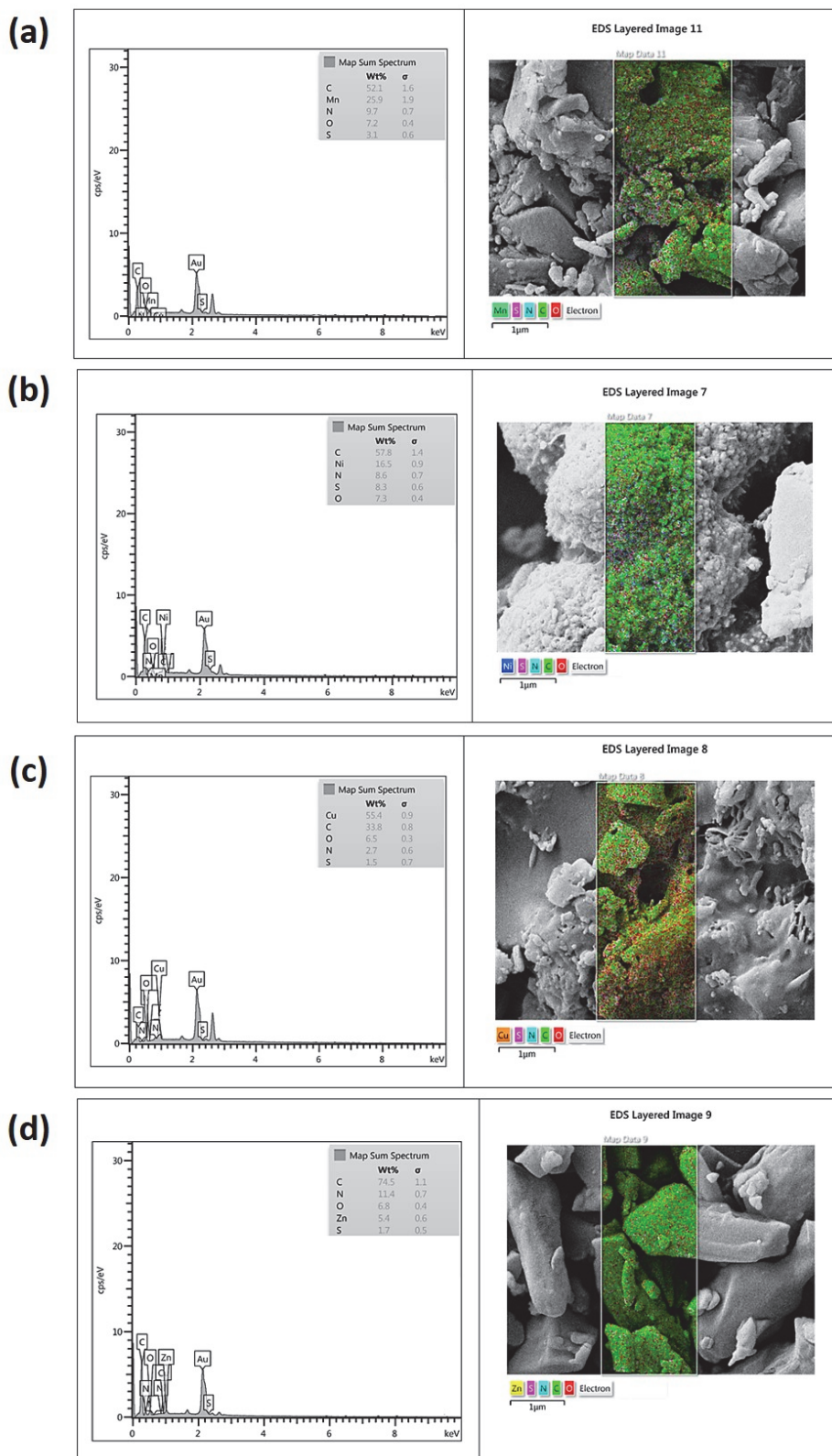
Figure 1. EDX mapping images of complexes containing (a) Mn, (b) Ni, (c) Cu, and (d) Zn.

Surface morphology of 5–8

The morphology, particle sizes, and porosity of metal complexes **5–8** were examined using various microscopy techniques. FESEM provided clear and undistorted images of the surface of complexes **5–8** (Figure 2). FESEM images indicate the uniformity, amorphous nature, and roughness of surfaces. The

roughness of the surface can influence the adsorption of CO_2. The increase in the roughness of materials leads to a greater surface area for gas adsorption [62]. In addition, the FESEM images showed the existence of a range of particle sizes. Complexes **5–8** have irregular pore sizes with particle diameters in the range of 37–189, 35–69, 31–263, and 26–241 nm for the complexes containing Mn, Ni, Cu, and Zn, respectively [63].
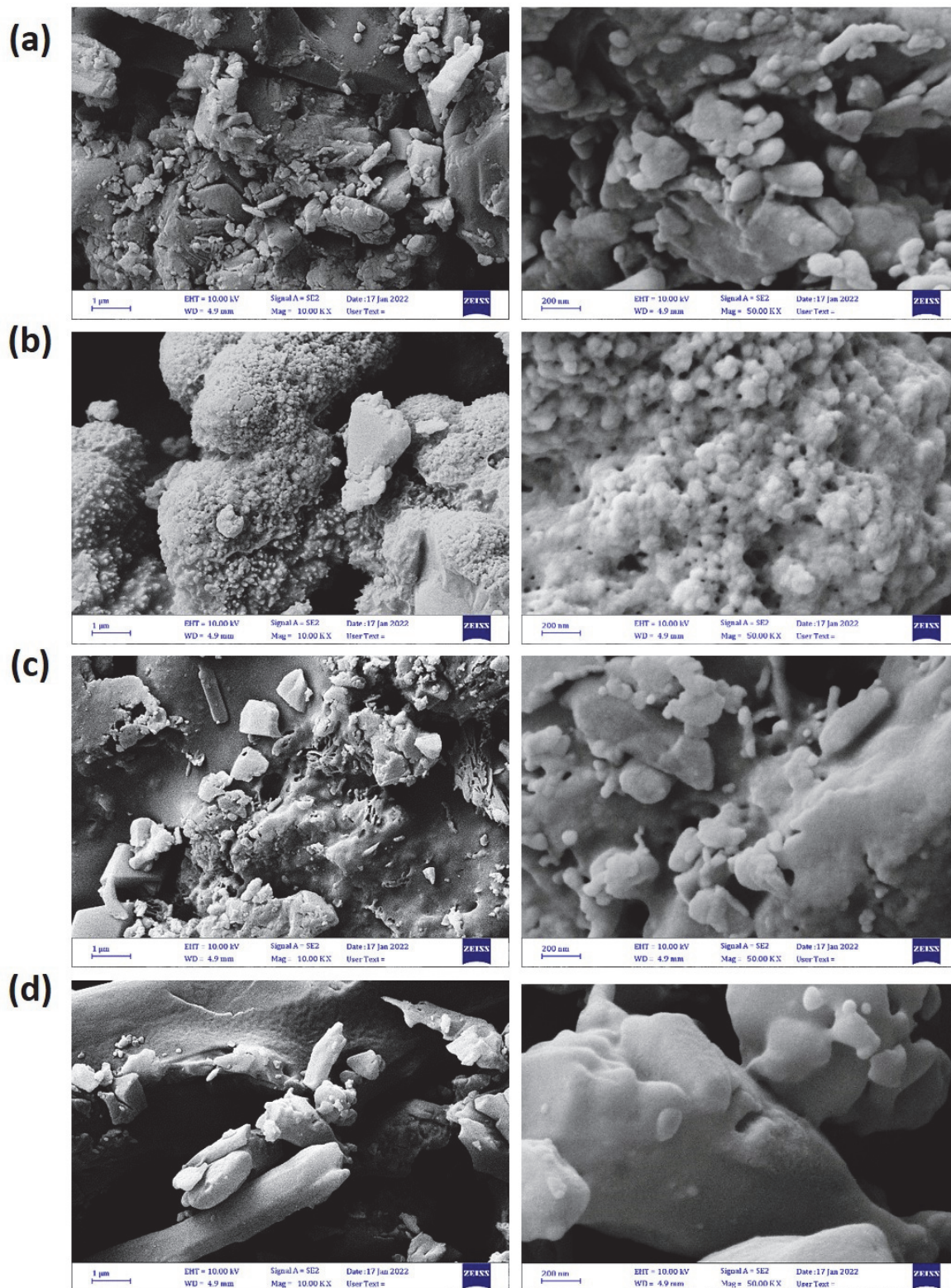

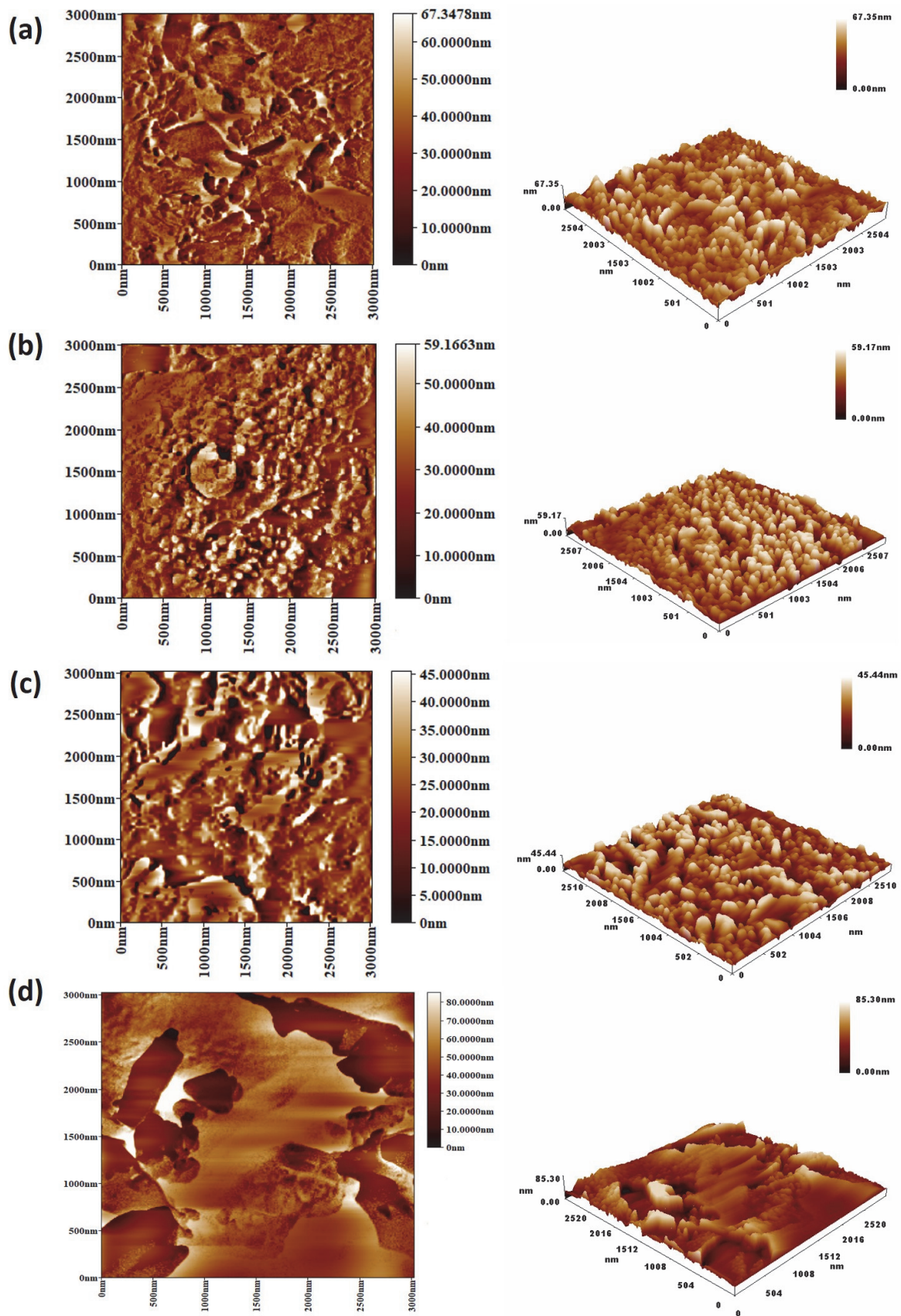*Figure 2. FESEM image of complexes containing (a) Mn, (b) Ni, (c) Cu, and (d) Zn.*

Figure 3. AFM images of complexes containing (a) Mn, (b) Ni, (c) Cu, and (d) Zn.

The AFM (two and three-dimensional) images provided information about the surface porosity and roughness (Figure 3). The AFM images indicated that the surface of the metal complexes is rough and highly porous. The roughness factor for the surface of metal complexes containing Mn, Ni, Cu, and Zn was 356, 175, 124, and 238, respectively. The particle sizes were 31.3–207.8, 33.5–117.5, 83.7–386.6, and 67.0–460.9 nm for complexes containing Mn, Ni, Cu, and Zn, respectively. It was clear that the particle sizes measured by the AFM in the Cu and Zn-based samples were more or less correlated with those obtained from the FESEM. However, the AFM provides much larger particle sizes in the Cu and Zn complex-es compared to those provided by the FESEM. It is not clear why this variation took place, but it could be that the particle sizes were just visually estimated from the FESEM.

The BET surface area of 5–8

The BET surface area determines the adsorption capacity of adsorbents, and additionally, the porosity provides information about their chemical and physical interactions with the adsorbed gas. Therefore, the nitrogen isotherms, along with the pore size distribution of complexes containing Mn, Ni, Cu, and Zn, were determined (Figure 4).
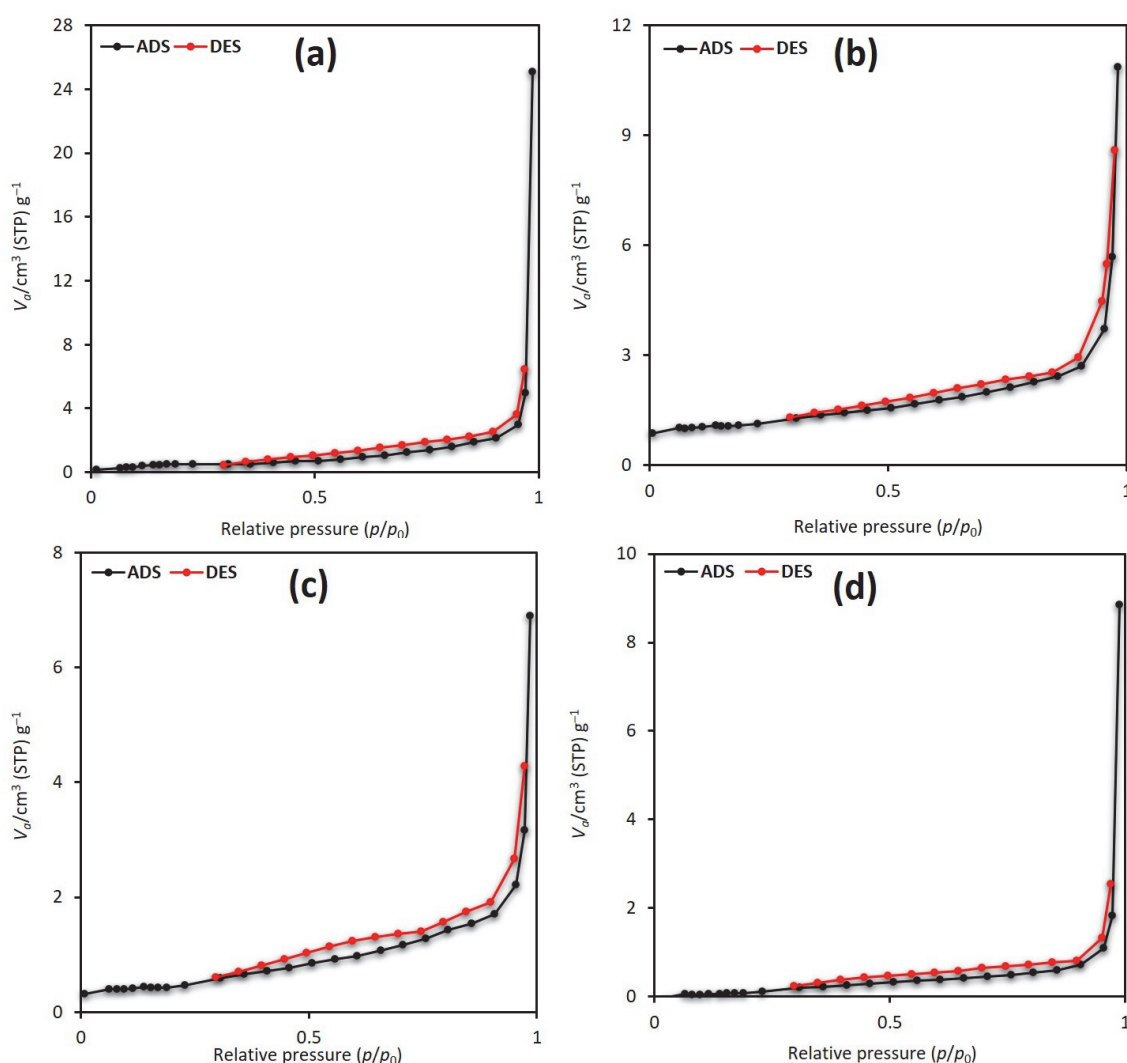

Figure 4. The N2 adsorption isotherms of complexes containing (a) Mn, (b) Ni, (c) Cu, and (d) Zn.

The interactions between the metal complexes and CO_2 were relatively weak [64]. The isotherms indicated that the structures of complexes are type IV mesoporous. No identifiable monolayer formation was found. The nitrogen adsorption isotherms ($P/P^o = 0.9$) were used to calculate the BET surface area and pore volume. The desorption data was used to estimate the average pore diameter (Table 5). The BET surface area of metal complexes was low (1.20–4.01 m²/g), and the pore volume and diameter were in the ranges

0.011–0.039 cm³/g and 16.77–97.62 nm, respectively. The Mn complex has the highest BET surface area (4.01 m²/g), pore volume (0.039 cm³/g), and diameter (97.62 nm). It seems likely that interparticle sorption takes place at the high relative pressure used, leading to a steep increase in the uptake graphs.

Table 5. Surface area and pore size distribution of metal complexes obtained by the N2 adsorption

Com-plex	Metal	S_{BET} (m²/g)	Pore volume (cm³/g)	Average pore diameter (nm)
5	Mn	4.01	0.039	97.62
6	Ni	1.20	0.011	16.77
7	Cu	1.59	0.014	26.30
8	Zn	1.62	0.017	45.77

The CO_2 uptake of 5–8

The pores' size and the type and strength of interactions between adsorbent and CO_2 (e.g., Van der Waal forces or hydrogen bonding) control CO_2 adsorption. High energy is required to adsorb CO_2 if the aperture size is small compared to the molecular size,

as repulsive forces could dominate [65]. In addition, the effect of pores' volume of absorbent materials is important for gas uptake capacity [66], with materials with large pores volumes having the space to store more CO_2 [67]. The chosen conditions for the CO_2 uptake process were based on our previous related work [45–53]. The CO_2 uptake recorded at 323 K and 40 bars for the complexes containing Mn, Ni, Cu, and Zn were 13.1, 10.1, 4.3, and 10.8 cm³/g, respectively (Figure 5). In terms of wt %, the CO_2 uptake was 2.6, 2.0, 0.9, and 2.1% for the Mn, Ni, Cu, and Zn complexes, respectively. The Mn complex led to the highest CO_2 uptake compared to the others. The Mn complex has the highest BET surface area and pore volume and diameter. In addition, the Mn atom has the lowest atomic radii compared with the other metals. Generally, the CO_2 uptake by complexes is reasonable since the complexes have a small surface area. This provides a sound starting point for the optimization of the chemical and physical properties to improve the interactions and capacity of the materials. We have not attempted to study the stability of the complexes. However, we believe they are highly stable since physisorption mainly takes place in the adsorption of CO_2. Therefore, the complexes should remain intact during and after the adsorption process.
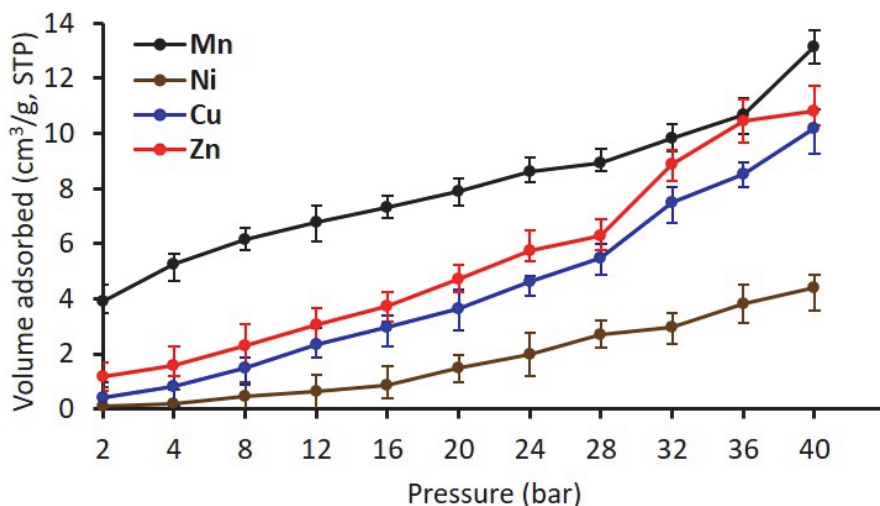

Figure 5. The CO2 adsorption isotherms for the metal complexes.

It is believed that the CO_2 adsorption mechanism is dependent on both the aromatic moieties, polarity of heteroatoms, and the Lewis acid center in the complexes used. We believe that physisorption is involved in CO_2 adsorption by the newly synthesized metal complexes. Physisorption plays an important role in the adsorption of gas due to the interaction between the polarized bonds within both the com-

plexes and CO_2 [68]. Table 6 shows the CO_2 uptake (wt %) over various storage media that have been reported recently in comparison to those achieved using the currently synthesized metal complexes. Clearly, multiple factors are controlling the adsorbent's efficacy toward CO_2 uptake. The most common factors are the surface area, pores volume and diameter, and surface morphology.

Table 6. Surface area and CO2 uptake of recently synthesized adsorbents

Adsorbent	S_{BET} (m²/g)	CO_2 (wt)	T (K), P (bar)	Ref
Thiophene-metal complexes	1.2–4.0	0.9–2.6	323, 40	Current
Polyphosphates–1,4-diaminobenzene	82.7–213.5	2.0–6.0	323, 40	45
Polysilicates	8.2–18.0	2.2–6.0	323, 40	46
Polyphosphates–benzidine	24.8–30.0	1.8–14.0	323, 50	47
Trimethoprim Schiff bases	4.2–20.3	6.0–10.3	313, 40	48
Melamine Schiff bases	5.2–11.6	6.1–10.0	323, 40	49
Metal-fusidate complexes	31.2–46.9	6.3–7.2	323, 50	50
Valsartan-metal complexes	16.0–22.8	4.8–6.8	323, 40	51
Carvedilol metal complexes	6.1–9.1	2.1–3.5	323, 40	52
Telmisartan metal complexes	32.4–130.4	3.3–7.1	323, 50	53

Conclusions

Four complexes containing heterocyclic units and metals were synthesized, and their structures were confirmed spectroscopically. Their physical properties and surface morphology were assessed. The materials have a diameter ranging from 16.77 to 97.62 nm and a specific surface area in the range of 1.20–4.01 m²/g. The highest CO_2 storage capacity was achieved with the complex containing manganese, followed by the others in the order of zinc, copper, and nickel. The manganese complex has the largest surface area, pores' volume, and average diameter compared with the others. In addition, the manganese-containing complex has the highest surface roughness factor. The results obtained open gates for designing a better storage media for CO_2. However, the toxicity that might be associated with these materials, their regeneration, and reuse need to be assessed.

Conflicts of Interest

The authors declare no conflict of interest requiring disclosure in this article.

REFERENCES

1. A.L. Yaumi, M.Z. Abu Bakar, B.H.Hameed (2017) Recent advances in functionalized composite solid materials for carbon dioxide capture. Energy, 124, 461–480, https://doi.org/10.1016/j.energy.2017.02.053

2. A. Mardani, D. Streimikiene, F. Cavallaro, N. Loganathan, M. Khoshnoudi (2019) Carbon dioxide (CO_2) emissions and economic growth: a systematic review of two decades of research from 1995 to 2017. *Sci. Total Environ.*, 649, 31–49, https://doi.org/10.1016/j.scitotenv.2018.08.229.

3. H.Sun, Q.Xin, Z.Ma, S.Lan (2019) Effects of plant diversity on carbon dioxide emissions and carbon removal in laboratory-scale constructed wetland. *Environ. Sci. Pollut. Res.*, 26, 5076–5082, https://doi.org/10.1007/s11356-018-3988-5.

4. K. B. Boamah, J. Du, I. A. Bediako, A. J. Boamah, A. A. Abdul-Rasheed, S. M. Owusu (2017) Carbon dioxide emission and economic growth of China–the role of international trade. *Environ. Sci. Pollut. Res.*, 24, 13049–13067, https://doi.org/10.1007/s11356-017-8955-z.

5. E. S. Sanz-Pérez, C. R. Murdock, S. A. Didas, C. W. Jones (2016) Direct capture of CO_2 from ambient air. *Chem. Rev.*, 116, 11840–11876, https://doi.org/10.1021/acs.chemrev.6b00173.

6. Z. Liu, Z. Deng, S. J Davis, C. Giron, P. Ciais (2022) Monitoring global carbon emissions in 2021. *Nat. Rev. Earth Environ.*, 3, 217–219, https://doi.org/10.1038/s43017-022-00285-w.

7. A.Qazi, F.Hussain, N.A.Rahim, G.Hardaker, D. Alghazzawi, K. Shaban, K. Haruna (2019) Towards sustainable energy: a systematic review of renewable energy sources, technologies, and public opinions. *IEEE Access*, 7, 63837, https://doi.org/10.1109/ACCESS.2019.2906402.

8. N. A. Ludin, N. I. Mustafa, M.M. Hanafiah, M. A. Ibrahim, M. A. Teridi, S. Sepeai, A. Zaharim, K. Sopian (2018) Prospects of life cycle assessment of renewable energy from solar photovoltaic technologies: a review. *Renew. Sust. Energ. Rev.*, 96, 11–28, https://doi.org/10.1016/j.rser.2018.07.048.

9. Y. Ouyang, H. Yang, P. Zhang, Y. Wang, S. Kaur, X. Zhu, Z. Wang, Y. Sun, W. Hong, Y. F. Ngeow, H. Wang (2017) Synthesis of 2,4-diaminopyrimidine core-based

derivatives and biological evaluation of their anti-tubercular activities. *Molecules*, 22, 1592, https://doi.org/10.3390/molecules22101592.

10. A. I. Osman, M. Hefny, M. I. Maksoud, A. M. Elgarahy, D. W. Rooney (2021) Recent advances in carbon capture storage and utilisation technologies: a review. *Environ. Chem. Lett.*, 19, 797–849, https://doi.org/10.1007/s10311-020-01133-3.

11. T. Wilberforce, A. Olabi, E. T. Sayed, K. Elsaid, M. A. Abdelkareem (2021) Progress in carbon capture technologies. *Sci. Total. Environ.*, 761, 143203, https://doi.org/10.1016/j.scitotenv.2020.143203.

12. O. Jankovský, M. Lojka, A. M. Lauermannová, F. Antončík, M. Pavlík, D. Sedmidubský (2020) Carbon dioxide uptake by MOC-based materials. *Appl. Sci.*, 10, 2254., https://doi.org/10.3390/app10072254.

13. K. Goh, H. E. Karahan, E. Yang, T. H. Bae (2019) Graphene-based membranes for CO_2/CH_4 separation: key challenges and perspectives. *Appl. Sci.*, 2784. https://doi.org/10.3390/app9142784.

14. I. S. Omodolor, H. O. Otor, J. A. Andonegui, B. J. Allen, A. C. Alba-Rubio (2020) Dual-function materials for CO2 capture and conversion: a review. *Ind. Eng. Chem. Res.*,59, 17612–17631, https://doi.org/10.1021/acs.iecr.0c02218.

15. H. Muslemani, X. Liang, K. Kaesehage, J. Wilson (2020) Business models for carbon capture, utilization and storage technologies in the steel sector: a qualitative multi-method study. *Processes*, 8, 576, https://doi.org/10.3390/pr8050576.

16. S. F. Cannone, A. Lanzini, M. A Santarelli (2021) Review: on CO_2 capture technologies with focus on CO_2-enhanced methane recovery from hydrates. *Energies*, 14, 387, https://doi.org/10.3390/en14020387.

17. S. Shukrullah, M. Y. Naz, N. M. Mohamed, K. A. Ibrahim, N. M. Abdel-Salam, A. Ghaffar, (2019) CVD synthesis, functionalization and CO_2 adsorption attributes of multiwalled carbon nanotubes, *Processes*, 7, 634, https://doi.org/10.3390/pr7090634.

18. J. Li, Y. Hou, P. Wang, B. Yang (2019) A review of carbon capture and storage project investment and operational decision-making based on bibliometrics. *Energies*, 12, 23, https://doi.org/10.3390/en12010023.

19. A. Raza, R. Gholami, R. Rezaee, V. Rasouli, M. Rabiei (2019) Significant aspects of carbon capture and storage—a review. *Petroleum*, 5, 335–340, https://doi.org/10.1016/j.petlm.2018.12.007.

20. E. Schuler,M. Morana, N. R. Shiju, G. J. Gruter (2022) A new way to make oxalic acid from CO_2 and alkali formats: using the active carbonite intermediate. *Sustain. Chem. Clim. Action*, 1, 100001, https://doi.org/10.1016/j.scca.2022.100001.

21. S. Builes, P. López-Aranguren, J. Fraile, L .F. Vega, C. Domingo (2015) Analysis of CO_2 adsorption in amine-functionalized porous silicas by molecular simulations. *Energy Fuels*, 29, 3855–3862, https://doi.org/10.1021/acs.energyfuels.5b00781.

22. D. M. D'Alessandro, B. Smit, J. R. Long (2010) Carbon dioxide capture: prospects for new materials. *Angew. Chem. Int. Ed.*, 49, 6058–6082, https://doi.org/10.1002/anie.201000431.

23. A.Mukherjee, J.A.Okolie, A.Abdelrasoul, C.Niu, A.K.Dalai (2019) Review of post-combustion carbon dioxide capture technologies using activated carbon. *J. Environ. Sci.*, 83, 46–63, https://doi.org/10.1016/j.jes.2019.03.014.

24. A. A. Okesola, A. A. Oyedeji, A. F. Abdulhamid, J. Olowo, B. E. Ayodele, T. W. Alabi (2018) Direct air capture: A review of carbon dioxide capture from the air. *IOP Conf. Ser: Mater. Sci. Eng.*, 413, 012077, https://doi.org/10.1088/1757-899x/413/1/012077.

25. Z. Asadi-Sangachini, M.M. Galangash, H. Younesi, M. Nowrouzi (2019) The feasibility of cost-effective manufacturing activated carbon derived from walnut shells for large-scale CO_2 capture. *Environ. Sci. Pollut. Res.*, 26, 26542–26552, https://doi.org/10.1007/s11356-019-05842-3.

26. J. A. Gibson, E. Mangano, E. Shiko, A. G. Greenaway, A. V. Gromov, M. M. Lozinska, D. Friedrich, E.B. Campbell, P. A. Wright, S. Brandani (2016) Adsorption materials and processes for carbon capture from gas-fired power plants: AMPGas. *Ind.Eng.Chem.Res.*, 55, 3840– 3851,https://doi.org/10.1021/acs.iecr.5b05015.

27. S. Y. Lee, S. J. Park (2015) A review on solid adsorbents for carbon dioxide capture. *J. Ind. Eng. Chem.*, 23, 1–11, https://doi.org/10.1016/j.jiec.2014.09.001.

28. K. Sumida, D.L. Rogow, J. A. Mason, T. M. McDonald, E. D. Bloch, Z. R. Herm, T. H. Bae, J. R. Long (2012) A review on solid adsorbents for carbon dioxide capture. *Chem. Rev.*, 112, 724–781, https://doi.org/10.1021/cr2003272.

29. C. Lu, T. Ben, S. Qiu (2016) Synthesis and gas storage application of hierarchically porous materials. *Macromol.Chem.Phys*., 217, 1995– 2003, https://doi.org/10.1002/macp.201600221.

30. Japip, H. Wang, Y. Xiao, T. S. Chung (2014) Highly permeable zeolitic imidazolate framework (ZIF)-71 nano-particles enhanced polyimide membranes for gas separation. *J. Membr. Sci.*, 467, 162–174. https://doi.org/10.1016/j.memsci.2014.05.025.

31. Q. Huang, M. Eić (2013) Commercial adsorbents as benchmark materials for separation of carbon dioxide and nitrogen by vacuum swing adsorption process. *Sep. Purif. Technol.*, 103, 203–215, https://doi.org/10.1016/j.seppur.2012.10.040.

32. A. Ö. Yazaydın, A. I. Benin, S. A. Faheem, P. Jakubczak, J. J. Low, R. R. Willis, R. Q. Snurr (2019) Enhanced CO_2 adsorption in metal-organic frameworks via occupation of open-metal sites by coordinated water molecules. *Chem. Mater.*, 21, 1425–1430, https://doi.org/10.1021/cm900049x.

33. S. C. Lee, H. J. Chae, S. J. Lee, B. Y. Choi, C. K. Yi, J. B. Lee, C. K. Ryu, J. C. Kim (2008) Development of regenerable MgO-based sorbent promoted with K_2CO_3 for CO_2 capture at low temperatures. *Environ. Sci. Technol.*, 42, 2736–2741, https://doi.org/10.1021/es702693c.

34. S. Wang, S. Yan, X Ma, J. Gong (2011) Recent advances in capture of carbon dioxide using alkali-metal-based oxides. *Energy Environ. Sci*., 4, 3805–3819, https://doi.org/10.1039/c1ee01116b.

35. L. Hauchhum, P. Mahanta (2014) Carbon dioxide adsorption on zeolites and activated carbon by pressure swing adsorption in a fixed bed. *Int. J. Energy Environ. Eng.*, 5, 349–356, https://doi.org/10.1007/s40095-014-0131-3.

36. P. Staciwa, U. Narkiewicz, D. Sibera, D. Moszyński, R. J. Wróbel, R. D. Cormia (2019) Carbon spheres as CO_2 sorbents. *Appl. Sci.*, 9, 3349, https://doi.org/10.3390/app9163349.

37. A. S. Aquino, M. O. Vieira, A. S. Ferreira, E. J. Cabrita, S. Einloft, M. O. De Souza (2019) Hybrid ionic liquid–silica xerogels applied in CO_2 capture. *Appl. Sci.*, 9, 2614, https://doi.org/10.3390/app9132614.

38. Y. -C. Chiang, C. -Y Yeh, C. -H. Weng (2019) Carbon dioxide adsorption on porous and functionalized activated carbon fibers. *Appl. Sci.*, 9, 1977, https://doi.org/10.3390/app9101977.

39. J. Choma, M. Kloske, A. Dziura, K. Stachurska, M. Jaroniec (2016) Preparation and studies of adsorption properties of microporous carbon spheres. *Eng. Prot. Environ.*, 19, 169–182, https://doi.org/10.17512/ios.2016.2.1.

40. R. Dawson, A. I. Cooper, D. J. Adams (2012) Nanoporous organic polymer networks. *Prog. Polym. Sci.*, 37, 530–563, https://doi.org/10.1016/j.progpolymsci.2011.09.002.

41. S. Choi, J. H. Drese, C. W. Jones (2009) Adsorbent materials for carbon dioxide capture from large anthropogenic point sources. *ChemSusChem*, 2, 796–854, https://doi.org/10.1002/cssc.200900036.

42. W. Wang, M. Zhou, D. Yuan (2017) Carbon dioxide capture in amorphous porous organic polymers. *J. Mater. Chem. A*, 5, 1334–1347, https://doi.org/10.1039/c6ta09234a.

43. S. E. M. Elhenawy, M. Khraisheh, F. AlMomani, G. Walker (2020) Metal-organic frameworks as a platform for CO_2 capture and chemical processes: adsorption, membrane separation, catalytic-conversion, and electrochemical reduction of CO_2. *Catalysts*, 10, 1293, https://doi.org/10.3390/catal10111293.

44. P. Kumar, B. Anand, Y. F. Tsang, K. -H. Kim, S. Khullar, B. Wang (2019) Regeneration, degradation, and toxicity effect of MOFs: opportunities and challenges. *Environ. Res.*, 176, 108488, https://doi.org/10.1016/j.envres.2019.05.019.

45. H. A. Satar, A. A. Ahmed, E. Yousif, D. S. Ahmed, M. F. Alotibi, G. A. El-Hiti (2019) Synthesis of novel heteroatom-doped porous-organic polymers as environmentally efficient media for carbon dioxide storage. *Appl. Sci.*, 9, 4314, https://doi.org/10.3390/app9204314.

46. S.H., Mohamed, A. S. Hameed, E. Yousif, M. H. Alotaibi, D. S. Ahmed, G. A. El-Hiti (2020) New porous silicon-containing organic polymers: synthesis and carbon dioxide uptake. *Processes*, 8, 1488, https://doi.org/10.3390/pr8111488.

47. D. S. Ahmed, G. A. El-Hiti, E. Yousif, A. S. Hameed, M. Abdalla (2017) New eco-friendly phosphorus organic polymers as gas storage media. *Polymers*, 9, 336, https://doi.org/10.3390/polym9080336.

48. A. A. Yaseen, E. T. B. Al-Tikrity, G. A. El-Hiti, D.S.Ahmed, M.A.Baashen, M.H. Al-Mashhadani, E. Yousif (2021) A process for carbon dioxide capture using Schiff bases containing a trimethoprim unit. *Processes*, 9, 707, https://doi.org/10.3390/pr9040707.

49. R. M. Omer, E. T. B. Al-Tikrity, G. A. El-Hiti, M. F. Alotibi, D. S Ahmed, and E. Yousif (2020) Porous aromatic melamine Schiff bases as highly efficient media for carbon dioxide storage. *Processes*, 8, 17, https://doi.org/10.3390/pr8010017.

50. Z. N. Mahmood, M. Alias, G. A. -R. El-Hiti, D. S. Ahmed, E. Yousif (2021) Synthesis and use of new porous metal complexes containing a fusidate moiety as gas storage media. *Korean J. Chem. Eng.*, 38, 179–186, https://doi.org/10.1007/s11814-020-0692-1.

51. A. Mohammed, E. Yousif, and G. A. El-Hiti (2020) Synthesis and use of valsartan metal complexes as media for carbon dioxide storage. *Materials*, 13, 1183, https://doi.org/10.3390/ma13051183.

52. O. G. Mousa, E. Yousif, A. A. Ahmed, G. A. El-Hiti, M. H. Alotaibi, D. A. Ahmed (2020) Synthesis and use of carvedilol metal complexes as carbon dioxide storage media. *Appl. Petrochem. Res.*, 10, 157–164, https://doi.org/10.1007/s13203-020-00255-7.

53. A. G. Hadi, K. Jawad, E. Yousif, G. A. El-Hiti, Alotaibi, D. S. Ahmed (2019) Synthesis of telmisartan organotin(IV) complexes and their use as carbon dioxide capture media. *Molecules*, 24, 1631, https://doi.org/10.3390/molecules24081631.

54. M. Nakao, M. Toguchi, K. Horikoshi, S. Kitaike, S. Sano (2022) Synthesis of novel 2,3-disbstututed thiophenes via tandem thia-Michael/aldol reactions of allenyl esters. *Heterocycles*, 104, 379–388, https://doi.org/10.3987/COM-21-14575.

55. B. A. Baldo, N. H. Phan (2017) Drug Allergy: Clinical Aspects, Diagnosis, Mechanism, Structure–Activity Relationship; 2nd Ed., Springer Cham, London, UK, 134–162, https://doi.org/10.1007/978-3-030-51740-3.

56. A. J. Abdulghani, R. Kh. Hussain (2015) Synthesis and characterization of Schiff base metal complexes derived from cefotaxime with 1*H*-indole-2,3-dione (isatin) and 4-*N,N*-dimethylaminobenzaldehyde. *Open J. Inorg. Chem.*, 5, 83–101, https://doi.org/10.4236/ojic.2015.54010.

57. N. Hasani, M. N. A. Al-Jibouri (2017) Synthesis, characterization, and DFT study of some transition metal complexes with Schiff base derived from 2-acetylthiophene and L-methionine. *Res. Chem. Intermed.*, 43, 4585–4610, https://doi.org/10.1007/s11164-017-2898-3.

58. M. A. Ayoub, E. H. Abd-Elnasser, M. A. Ahmed, M. G. Rizk (2018) Some new metal(II) complexes based on bis-Schiff base ligand derived from 2-acetylethiophine and 2,6-diaminopyridine: synthesis, structural investigation, thermal, fluorescence and catalytic activity studies. *J. Mol. Struct.*, 1163, 379–387, https://doi.org/10.1016/j.molstruc.2018.03.006.

59. F. A. El-Saied, M. M. E. Shakdofa, A. S. El-Tabi, M. M. Abdel-Zaher, N. Morsy (2017) Coordination versatility of N_2O_4 polydentate hydrazonic ligand in Zn(II), Cu(II), Ni(II), Co(II), Mn(II), and Pd(II) complexes and antimicrobial evaluation. *Beni-Suef Univ. J. Basic Appl. Sci.*, 6, 310–320, https://doi.org/10.1016/j.bjbas.2017.09.005.

60. C. A. Housecroft, A. G. Sharpe (2012) Inorganic Chemistry; 4th Ed., Pearson Education Limited, England, UK, 1213 pp. ISBN 0273742752, 9780273742753.

61. H. O. Echekwube, P.O. Ukoha, O. T. Ujam, C. O. Nwuche, J. N. Asegbeloyin, A. Ibezim (2019) Synthesis and in silico investigation of Schiff base derivatives of 1H-indole-2,3-diones and their Co(II) and Ni(II) complexes as antimicrobial agents. *Braz. J. Biol. Sci.*, 6, 63–85, https://doi.org/10.21472/bjbs.061207.

62. X. Yu, K. Regenauer-Lieb, F. Tian (2019) Investigation of effects of surface roughness on coal seam gas transport using a fractal-based lattice Boltzmann method. *ASEG Extended Abstracts*, 1, 1–2, https://doi.org/10.1080/22020586.2019.12073014.

63. B. R. Vergis, N. Kottam, R. H. Krishna, B. N. Nagabhushana (2019) Removal of Evans Blue dye from aqueous solution using magnetic spinel $ZnFe_2O_4$ nanomaterial: adsorption isotherms and kinetics. *Nano-Struct. Nano-Objects*, 18, 100290, https://doi.org/10.1016/j.nanoso.2019.100290.

64. K. A. Cychosz, M. Thommes (2018) Progress in the physisorption characterization of nanoporous gas storage materials. *Engineering*, 4, 559–566, https://doi.org/10.1016/j.eng.2018.06.001.

65. H. Furukawa, O. M. Yaghi (2009) Storage of hydrogen, methane, and carbon dioxide in highly porous covalent organic frameworks for clean energy applications. *J. Am. Chem. Soc.*, 131, 8875–8883, https://doi.org/10.1021/ja9015765.

66. Y. Peng, V. Krungleviciute, I. Eryazici, J. T. Hupp, O. K. Farha, T. Yildirim (2013) Methane storage in metal–organic frameworks: current records, surprise findings, and challenges. *J. Am. Chem. Soc.*, 135, 11887–11894, https://doi.org/10.1021/ja4045289.

67. M. Razavian, S. Fatemi, M. A. Masoudi-Nejad (2014) Comparative study of CO2 and CH4 adsorption on silicalite-1 fabricated by sonication and conventional method. *Adsorpt. Sci. Technol.*, 32, 73–87, https://doi.org/10.1260/0263-6174.32.1.73.

68. A.A.Abd, S.Z.Naji, A.S.Hashim, M.R.Othman (2020) Carbon dioxide removal through physical adsorption using carbonaceous and non-carbonaceous adsorbents: a review. *J. Environ. Chem. Eng.*, 8, 104142, https://doi.org/10.1016/j.jece.2020.104142.

IZVOD

SINTEZA I SVOJSTVA NOVIH METALNIH KOMPLEKSA KOJI SADRŽE HETEROCIKLIČNE GRUPE I ISTRAŽIVANJE ULOGE METALA U HVATANJU GASA UGLJEN-DIOKSIDA

Kontinuirano oslobađanje ugljen-dioksida (CO_2) u atmosferu će neizbežno dovesti do veće štete po životnu sredinu. Sakupljanje i skladištenje CO_2 je jedna od strategija za ublažavanje štete povezane sa visokim koncentracijama CO_2 u atmosferi. Dizajn i sinteza novih materijala koji će delovati kao medij za skladištenje CO_2 je trenutno važan izazov za istraživače. S tim u vezi, objavljeno je istraživanje sinteze novih organometalnih materijala i njihovog potencijala kao medija za skladištenje CO_2. Stoga je trenutni rad imao za cilj da proizvede nove materijale koristeći jednostavnu proceduru i istraži njihova svojstva, uključujući faktore koji utiču na njihovu adsorpciju CO_2. Četiri metalna kompleksa koji sadrže heterociklične jedinice sintetizovana su jednostavnom metodom, a njihove strukture su potvrđene korišćenjem nekoliko tehnika. Morfologija površine materijala je pregledana mikroskopski. Metalni kompleksi su pokazali podesive veličine čestica sa prečnicima koji su se kretali od 16,77 do 97,62 nm i Brunauer-Emmett-Teller-ovom površinom od 1,20-4,01 m²/g. Materijali mogu uhvatiti CO_2 na 323 K i 40 bara, pri čemu kompleks koji sadrži mangan pokazuje najveći kapacitet skladištenja CO_2 (13,1 cm³/gm).

Ključne reči: *sinteza, metalni kompleksi, hvatanje ugljen-dioksida, površina, morfologija površine*

The ORCID Ids of all the authors are as follows:

1. Rawnaq Jima'a: https://orcid.org/0000-0002-3706-2227 [2]
2. Naser Shaalan: https://orcid.org/0000-0002-2875-5056
3. Muna Bufaroosha: https://orcid.org/0000-0003-4799-3356
4. Gamal A. El-Hiti: https://orcid.org/0000-0001-6675-3126
5. Benson M. Kariuki: https://orcid.org/0000-0002-8658-3897
6. Dina S. Ahmed: https://orcid.org/0000-0003-2205-4061
7. Emad Yousif: https://orcid.org/0000-0003-1458-4724